Global albedo change and radiative cooling from anthropogenic land cover change, 1700 to 2005 based on MODIS, land use harmonization, radiative kernels, and reanalysis

Bardan Ghimire[1,2], Christopher A. Williams[1], Jeffrey Masek[3], Feng Gao[4], Zhuosen Wang[5,6], Crystal Schaaf[5], and Tao He[7]

[1]Graduate School of Geography, Clark University, Worcester, Massachussetts, USA, [2]Earth Sciences Division, Lawrence Berkeley National Laboratory, Berkeley, California, USA, [3]NASA Goddard Space Flight Center, Greenbelt, Maryland, USA, [4]ARS, USDA, Beltsville, Maryland, USA, [5]School for the Environment, University of Massachusetts, Boston, Massachusetts, USA, [6]NASA Postdoctoral Program Fellow, NASA Goddard Space Flight Center, Greenbelt, Maryland, USA, [7]Department of Geographical Sciences, University of Maryland, College Park, Maryland, USA

Abstract Widespread anthropogenic land cover change over the last five centuries has influenced the global climate system through both biogeochemical and biophysical processes. Models indicate that warming from carbon emissions associated with land cover conversion has been partially offset by cooling from elevated albedo, but considerable uncertainty remains partly because of uncertainty in model treatments of albedo. This study incorporates a new spatially and temporally explicit, land cover specific albedo product derived from Moderate Resolution Imaging Spectroradiometer with a historical land use data set (Land Use Harmonization product) to provide more precise, observationally derived estimates of albedo impacts from anthropogenic land cover change with a complete range of data set specific uncertainty. The mean annual global albedo increase due to land cover change during 1700–2005 was estimated as 0.00106 ± 0.00008 (mean ± standard deviation), mainly driven by snow exposure due to land cover transitions from natural vegetation to agriculture. This translates to a top-of-atmosphere radiative cooling of $-0.15 \pm 0.1\,\mathrm{W\,m^{-2}}$ (mean ± standard deviation). Our estimate was in the middle of the Intergovernmental Panel on Climate Change Fifth Assessment Report range of -0.05 to $-0.25\,\mathrm{W\,m^{-2}}$ and incorporates variability in albedo within land cover classes.

1. Introduction

Humans have enacted large-scale transformation of the terrestrial biosphere over the past millennium [*Foley et al.*, 2005; *Steffen et al.*, 2005]. Anthropogenic land cover change is one of the leading factors contributing to widespread global environmental changes [*Turner et al.*, 2007]. Improved estimates of the extent and rates of land cover change at regional and global scales have recently become available [*Hurtt et al.*, 2011] but have not yet been widely used to quantify associated changes to the climate system.

Land cover conversion can alter climate via both biogeochemical processes (e.g., carbon cycling) and biophysical processes (e.g., albedo, evapotranspiration, and surface roughness) [*Bala et al.*, 2007; *Barnes and Roy*, 2010; *Bonan*, 2008; *Brovkin et al.*, 2006; *Fall et al.*, 2010; *Pongratz et al.*, 2010]. The overall climate effect of land cover change depends on the relative magnitude of these processes and can vary regionally [*Bala et al.*, 2007; *Betts et al.*, 2007; *Bonan*, 2008]. Global studies with models have demonstrated that deforestation in low-latitude tropical regions induce a net global warming effect because decreased evapotranspiration and increased carbon emissions outweigh the cooling caused by higher albedo. In contrast, at higher latitudes, the relative magnitudes are reversed, resulting in a net cooling effect [*Randerson et al.*, 2006]. This net cooling in higher latitudes is related to increased exposure of high-albedo winter snow associated with conversion from tall to short stature vegetation during deforestation or forest disturbance.

Past work quantifying the albedo consequences of global land cover change mostly used coarse-gridded (i.e., coarser than around 2° spatial resolution) climate models and hypothetical scenarios of albedo change [*Bala et al.*, 2007; *Betts et al.*, 2007; *Pongratz et al.*, 2009]. Recent Earth observing systems make it now possible to estimate albedo around the globe with space-based spectral observations [*Schaaf et al.*, 2002], yet only a few studies have brought this new data source to bear on the question of albedo impacts of land cover

change [*Myhre et al.*, 2005]. The Intergovernmental Panel on Climate Change (IPCC) Fourth Assessment Report (2007) and Fifth Assessment Report (2013) provide a best estimate of the albedo-induced cooling from historical land cover change at the global scale, with preindustrial to present cooling amounting to approximately $-0.2 \, \text{W m}^{-2}$ [*Intergovernmental Panel on Climate Change (IPCC)*, 2007] or $-0.15 \, \text{W m}^{-2}$ [*IPCC*, 2013]. However, the range of estimates is large, spanning 0 to $-0.5 \, \text{W m}^{-2}$ [*IPCC*, 2007] and -0.05 to $-0.25 \, \text{W m}^{-2}$ [*IPCC*, 2013], and improved estimates are needed to reduce this uncertainty.

While the main driver of these changes reflects transitions among a few categories, such as human-induced conversion of natural vegetation (e.g., shrubs, grass, and forests) to crops [*Matthews et al.*, 2003; *Myhre and Myhre*, 2003; *Myhre et al.*, 2005], there can be large variation in the associated preconversion and postconversion albedos. For example, the albedo of corn grown in United States differs from that of rice in India, and such variation has not been taken into account in most prior studies. As such, previous studies have tended to simplify variability in albedo within land cover classes [e.g., *Myhre and Myhre*, 2003; *Pongratz et al.*, 2009], which can arise from many factors including differences in snow properties, time since disturbance, within class variation in vegetation composition, and soil background. Prior work has also typically combined multiple finer land cover categories for determining land cover specific albedo [e.g., *Matthews et al.*, 2003]. These limitations can be partially overcome by the use of remotely sensed albedo to extract unique albedo values at each location (e.g., image pixel) for different land cover types, combined with the best available information on historical land cover and change data sets.

The purpose of this study is to provide more precise estimates of historical (1700–2005) land cover change impacts on surface albedo and associated top-of-atmosphere (TOA) radiative forcing. This is achieved by merging a new satellite-derived product describing regional-scale land cover specific albedo over the globe with a new, state-of-the-art land cover change data set, the Land Use Harmonization (LUH) product [*Hurtt et al.*, 2006, 2011].

2. Methods

This study estimates the impacts of global historical land cover change on surface albedo and TOA radiative forcing by integrating (1) historical land cover maps to determine the rate and distribution of land cover transitions around the globe and (2) look-up maps (LUMs) that relate albedo values to corresponding land cover types.

2.1. Historical Land Cover Maps

We have based our historical land cover trajectories on the Land Use Harmonization (LUH) product [*Hurtt et al.*, 2006; *Hurtt et al.*, 2011], which portrays the most probable land use for every 0.5° global cell since 1700. The land cover maps used in this study were generated by converting the LUH land use classes mapped from 1700 to 2005 into the 18 International Geosphere-Biosphere Programme (IGBP) land cover classes. This conversion was performed separately using two different satellite land cover products (namely, Moderate Resolution Imaging Spectroradiometer (MODIS) and Advanced Very High Resolution Radiometer (AVHRR)) generating two different historical land cover data sets that encompass the uncertainty in the mapping process. The LUH product was intersected with the IGBP 30 arc sec AVHRR land cover map [*Eidenshink and Faundeen*, 1994] for the common time period (1992–1993) between these two data sets. Prior to the intersection, the fraction of each land cover type described at 0.5° in the LUH product was converted to 1° by averaging across 2×2 pixel blocks (representing 1° spatial resolution) for each land cover type separately. The LUH product reports the fraction of five different broad land cover types in each pixel. A sixth LUH land cover class for water/ice was obtained by subtracting the sum of the fractional coverage of the five LUH land cover types from unity (one) for each pixel. Similarly, the 30 arc sec AVHRR land cover map was also converted to 1° by determining the proportion of pixels of a given land cover type within each 180×180 pixel block of 1° spatial resolution. Subsequently, the intersection of the LUH (averaged 1992 and 1993) map and 1992–1993 AVHRR land cover map was used to derive the one-to-one or one-to-many mapping of land cover classes for each pixel to convert each of the six broad land cover classes to one or more of the IGBP land cover categories for each pixel. This approach retains regional specificity in the translation of LUH classes such as secondary land to various IGBP cover classes.

The one-to-one and one-to-many land cover class mapping was specified for each pixel separately based on map intersection. In the one-to-one mapping, the LUH classes urban and croplands were directly and exclusively mapped to their corresponding IGBP class. The remaining four classes were mapped with a

one-to-many class relationship, where (a) LUH pasture was mapped to IGBP closed shrublands, open shrublands, woody savannas, savannas, and/or grasslands; (b) LUH primary and secondary lands were mapped to all IGBP forest types as well as closed shrublands, open shrublands, woody savannas, savannas, and/or grasslands; and (c) LUH water/ice was mapped to IGBP water bodies, wetlands, and/or snow and ice. Pixels lacking a particular one-to-many mapping were obtained from the nearest pixel. These IGBP matching fractions for each pixel were normalized to sum to unity. These relationships were assumed to be temporally invariant and were extrapolated in time by multiplying the LUH fractions with the normalized matching IGBP land cover proportions. After applying these relationships, proportional maps of each IGBP land cover type from 1700 to 2005 were obtained. The barren areas were kept constant from 1700 to 2005 based on the AVHRR land cover product because the LUH product does not explicitly represent barren areas, by aggregating barren class into primary and secondary land that also includes vegetation. To access the uncertainty in the land cover intersection, the entire analysis was repeated using MODIS land cover [*Friedl et al.*, 2002] instead of the AVHRR land cover product. The MODIS land cover was generated from the most frequently occurring land cover category from 2001 to 2005 in the MODIS product.

2.2. Albedo Look-Up Maps

Albedo look-up maps based on MODIS satellite data were used to determine the albedo values for a given land cover type, month, and location [*Gao et al.*, 2014]. These LUMs were derived by intersecting (1) the monthly composite (median albedo) MODIS broadband albedo product [*Schaaf et al.*, 2002] from 2001 to 2011 at 30 arc sec (~1 km) spatial resolution and 2) the climatology land cover (temporally frequently occurring class) from 2001 to 2011 in the 30 arc sec MODIS land cover product [*Friedl et al.*, 2002]. This intersection was performed for four unique pairwise combinations of sky conditions (white sky and black sky, described below) and snow cover (snow free and snow covered) to obtain white-sky snow-free LUMs, white-sky snow-covered LUMs, black-sky snow-free LUMs, and black-sky snow-covered LUMs for different months of the year (from climatology) and for land cover types. The mean LUMs were used in this study along with the mean plus standard deviation and mean minus standard deviation LUMs to assess uncertainty in the LUMs. Unlike traditional land cover/albedo look-up tables, the LUMs used in this study were geographically specific; that is, albedo for a given land cover type (such as cropland) can vary regionally to reflect the dominant vegetation type, soil background, or land management. Pixels in the LUMs that lacked a locally defined albedo for a specific class were filled with interpolation by averaging valid pixel values from progressively larger filter blocks until valid pixel values were found. In the worst case, algorithm may end up with the global statistics (same as the global look-up table). The LUMs were available at different spatial resolutions from 0.05 to 1°. The albedo LUMs were assessed by applying to the LUH cross-walked IGBP map in MODIS era (2001–2005). The modeled albedo show very good agreement with the MODIS albedo data product. Further details on the LUMs are available at *Gao et al.* [2014].

White-sky albedo is the ratio of upwelling to downwelling radiative flux at the surface for conditions of isotropic, diffuse illumination, whereas black-sky albedo refers to conditions of direct illumination only. Actual albedo was calculated from the sum of black-sky and white-sky components based on the relative intensity of diffuse and direct illumination. In this work, we relied on the common assumption of isotropic distribution of diffuse skylight. While this assumption can lead to local biases (particularly at higher solar zenith angles) because of multiple radiative interactions between the ground and atmosphere [*Pinty et al.*, 2005; *Román et al.*, 2010], we expect this to have a negligible effect for the current application.

2.3. Historical Land Cover Change Impacts on Surface Albedo and TOA Radiative Forcing

Albedo maps were calculated at 1° spatial resolution from 1700 to 2005 by applying the albedo LUMs to the 18 class historical land cover maps. Specifically, the LUMs and the IGBP based 18 class land cover maps were used to compute albedo (α) of each pixel for each month (m) and year (y):

$$\alpha_{m,y} = \sum_{l=0}^{17} \sum_{s=0}^{1} \sum_{r=0}^{1} f_{l,y} f_{s,m} f_{r,m} \propto_{l,s,r,m} \tag{1}$$

where $f_{l,y}$ was the fraction (f) for a given land cover class (l) at year (y), f_s was the fraction for snow-covered ($s = 0$) and snow-free ($s = 1$) conditions at month (m), and f_r was the fraction for white-sky ($r = 0$) and black-sky ($r = 1$) radiation conditions at month (m). The snow-covered and snow-free fractions were derived from the 0.05° spatial resolution monthly level 3 MODIS terra snow cover climate modeling grid global product [*Hall et al.*, 2002] averaged from 2001 to 2011, resampled to 1° spatial resolution. Lacking readily available

historical snow cover data for the globe, this study was forced to adopt an assumption of stationarity in the snow-covered climatology for the full historical period of study. The white-sky and black-sky fractions were computed from the climatology of the mean monthly National Center for Atmospheric Research (NCAR) National Centers for Environmental Prediction (NCEP) diffuse and beam incoming surface solar (visible plus near-infrared) radiation reanalysis Gaussian grid (T62 with 94 × 192 points) product [*Kalnay et al.*, 1996; *Kistler et al.*, 2001] from 1981 to 2010. For the same reason as above, we also assume radiation fields are stationary over time.

TOA radiative forcing (*F*) of each pixel was computed using albedo radiative kernels (*K*) generated by *Shell et al.* [2008] and albedo change (Δ*α*) maps for diffuse/white-sky (*ws*) and direct/black-sky (*bs*) radiation conditions from 1700 to 2005, assuming 1700 as the reference year:

$$F_{m,y} = \Delta\alpha_{m,y,ws}K_{ws} + \Delta\alpha_{m,y,bs}K_{bs} \qquad (2)$$

The albedo radiative kernels specify the ratio of TOA radiative forcing (i.e., change in the TOA balance of the outgoing and absorbed radiation) to the surface albedo change. As a result, multiplication of the radiative kernels (*K*) with surface albedo change (Δ*α*) was performed to estimate radiative forcing. This multiplication of radiative kernels and surface albedo is performed separately for diffuse/white-sky conditions and direct/black-sky conditions to incorporate heterogeneity in radiation regimes, and subsequently, these two separate contributions were added to estimate the total radiative forcing (see equation (2)). The radiative kernels used in this study were derived from an off-line radiative transfer version of the Community Atmosphere Model version 3 [*Shell et al.*, 2008]. We did not use the blue-sky albedo computed from equation (1) to determine radiative forcing in equation (2). Instead, we used the white-sky and black-sky albedos because the kernels were specific for white-sky and black-sky conditions and would incorporate the heterogeneity in radiation regimes. To access the uncertainty in the different data products, we repeated the analysis for different combinations of the data products by substituting the Community Climate System Model version 4 snow cover product [*Lawrence et al.*, 2012] for the MODIS product, Modern-Era Retrospective Analysis for Research and Applications solar radiation product [*Rienecker et al.*, 2011] for the NCAR NCEP product, and Soden radiative kernel product [*Soden et al.*, 2008] for the product of *Shell et al.* [2008].
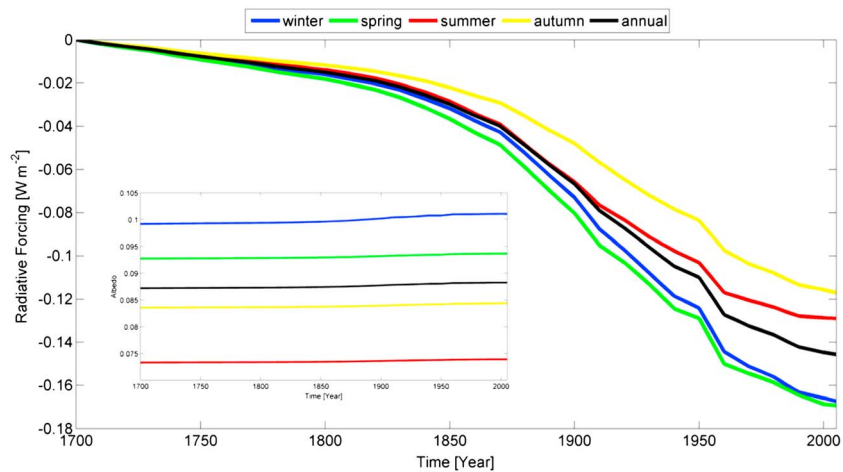
3. Results

The overall global trends in land cover from 1700 to 2005 show a large increase in croplands, and corresponding decrease in natural vegetation types, mainly forests and grasslands (Figures Sa1 and Sa2 and Tables Sa1 and Sa2 in the supporting information). The largest decrease in area was for mixed forest which decreased from 10% of global land area in 1700 to 7% in 2000 for the LUH AVHRR data set combination and decreased from 7% to 4% for the LUH MODIS data set combination. Evergreen broadleaf forest decreased from 9% to 7% for both the LUH AVHRR and LUH MODIS data set combination, and open shrublands decreased from 17% to 16% of land area for the LUH AVHRR data set combination and 16% to 15% for the LUH MODIS data set combination during the same time period. In contrast the largest gain in area was for croplands, which increased from 2% in 1700 to 9% in 2000 for both the LUH AVHRR and LUH MODIS data set combinations. This conforms to the well-known historical pattern of clearing natural vegetation to provide land for crops to meet the rising demand for food, fiber, and biofuel as human populations surged. The major hot spots of land cover change were in the North American, European, South Asian agricultural belts, and Sahelian Africa (Figure 1). Examples of hot spots of land cover change include forest to cropland with snow cover in Alberta, Canada (112 W, 53 N); South Dakota, U.S. (97 W, 44 N) and Russia south of Nizhny Novgorod (44 E, 54 N); and savanna or shrubland to cropland in Sudan southwest of El Obeid (28 E, 11 N) and India west of Kolkata (85 E, 25 N).

Land cover types exhibit large seasonal variability in albedo. The mean global surface albedo from different data product combinations was highest during northern hemisphere winter and lowest in northern hemisphere summer because of the high surface albedo of snow (Figure 2). The mean annual albedo trend from different data combinations was intermediate, averaging these trends across the year. Seasonal variation in the change of surface albedo due to land cover change can be large, with winter having the largest mean albedo increase from different data combinations of 0.00188 followed by spring (Δalbedo = 0.00093), autumn (Δalbedo = 0.00081), and summer (Δalbedo = 0.00060), each averaged over the globe (Figure 2). The largest mean albedo increase from different data combinations was observed in winter because the conversion of high stature vegetation
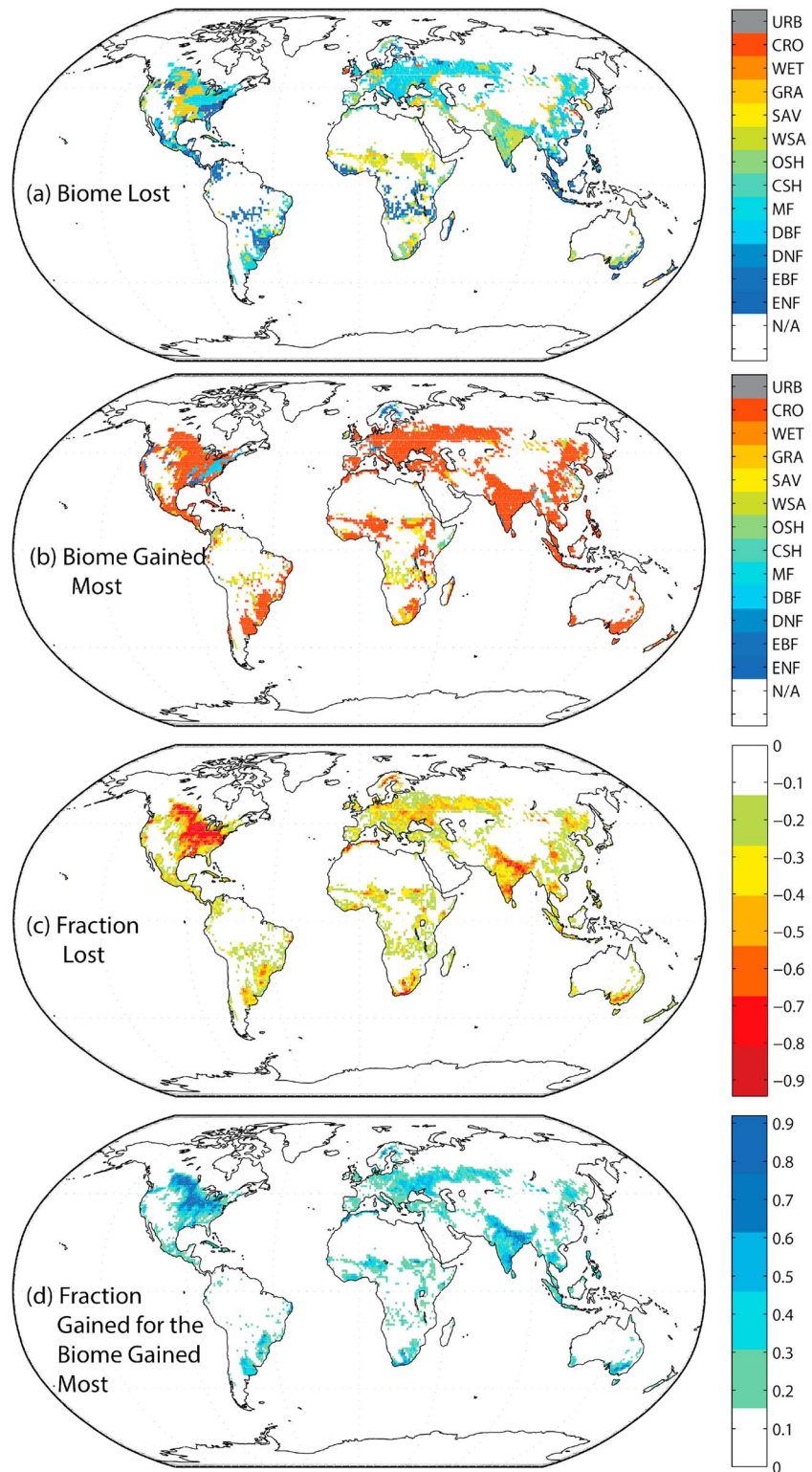
Figure 1. Spatial patterns of (a) fraction converted, (b) fractional gain for the land cover type gained most, (c) land cover type lost, and (d) land cover type gained most from 1700 to 2000 estimated from LUH and AVHRR.
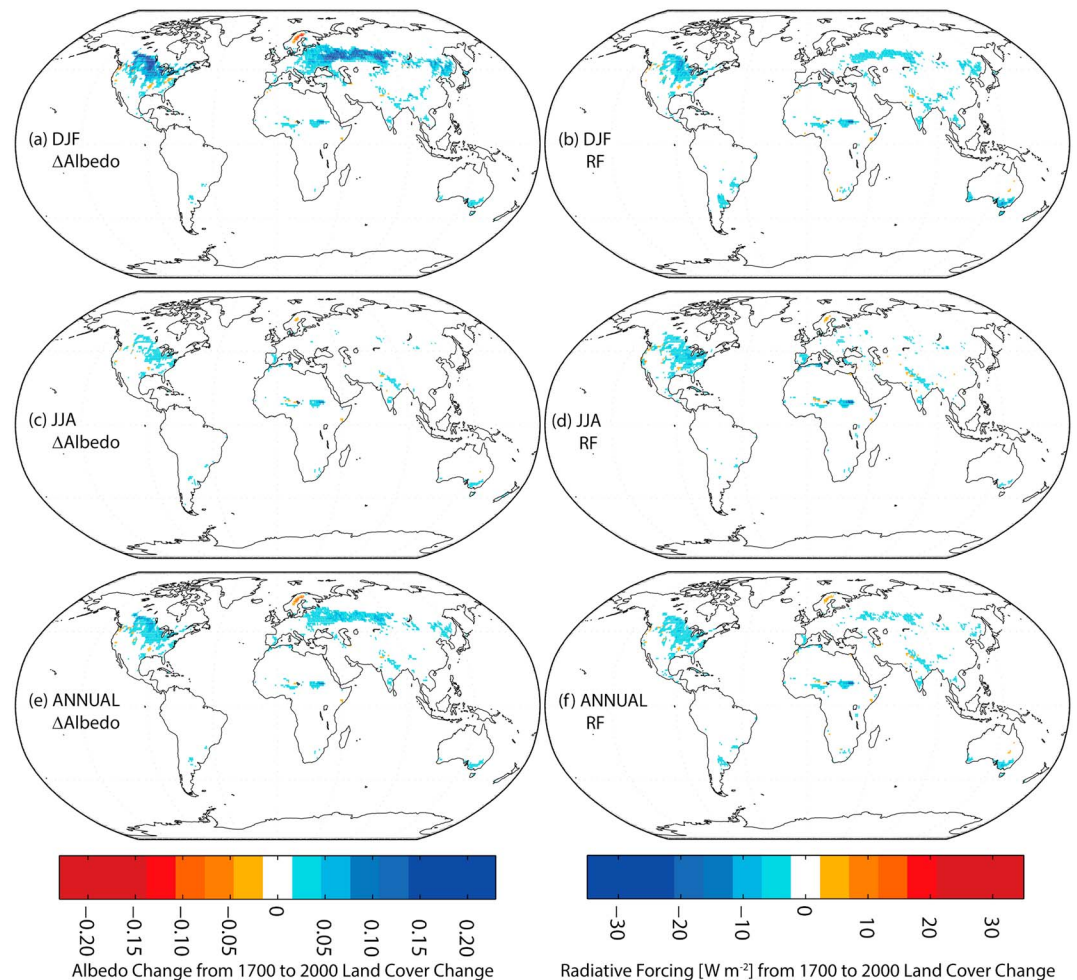
Figure 2. Global temporal trends in (a) albedo and (b) radiative forcing (W m^{-2}) due to historical land cover change from 1700 to 2005 estimated from average of different data set combinations.

(e.g., forests) to low stature vegetation (e.g., crops) results in snow exposure (see the supporting information for a table highlighting continental variations in land cover specific albedos by season and snow condition). The mean global annual increase in surface albedo from different data combinations aggregated across all seasons was 0.00106 ± 0.00008 (mean $\pm$ standard deviation) from 1700 to 2005 but can be much larger at local scales. Hot spot regions of large albedo change (Figure 3) can be seen in North America, Europe, South Asia, and the Sahel largely due to conversion to agriculture. In general, the magnitude of the spatial pattern of albedo change was larger in the high latitudes and in winter because of high snow cover in these regions in winter months.

The mean global annual TOA radiative forcing change from different data combinations aggregated across seasons was -0.15 W m^{-2} (cooling) from 1700 to 2005 (Figure 2) with standard deviation of 0.01 W m^{-2} and range of -0.13 W m^{-2} to -0.16 W m^{-2}. In general, the spatial patterns of global trends in surface albedo were similar to TOA radiative forcing trends (Figure 3). The mean radiative forcing changes from different data combinations vary by season with winter and spring seasons having similarly large magnitudes of radiative forcing change of -0.17 W m^{-2} (cooling) from 1700 to 2005 followed by summer (-0.13 W m^{-2}) and autumn (-0.12 W m^{-2}) (Figure 2). Although northern hemisphere winter season had the highest mean albedo difference (i.e., increase) compared to other seasons, this difference is reduced in the mean radiative forcing magnitudes. This is mainly because the TOA radiative forcing for the same albedo change was lower in northern hemisphere winter season compared to nonwinter because of lower radiative kernel values in higher latitudes in winter. The lower radiative kernels values were primarily caused by lower solar insolation in northern hemisphere winter season in higher latitudes.

4. Discussions and Conclusion

The mean TOA radiative forcing of -0.15 ± 0.01 W m^{-2} (cooling) from different data combinations due to land cover change from 1700 to 2005 estimated in this study indicates a cooling approximately equal to the mean of 0.15 W m^{-2} calculated from four different studies (Table 1) [*Betts et al.*, 2007; *Brovkin et al.*, 2006; *Myhre et al.*, 2005; *Pongratz et al.*, 2009] but falls approximately in the lower end of the range reported in the IPCC Fourth Assessment Report [*IPCC*, 2007] and in the middle of the range given in the IPCC Fifth Assessment Report [*IPCC*, 2013]. The main difference between our study and those prior was the use of new historical land cover reconstructions based on the LUH product [*Hurtt et al.*, 2006, 2011] and geographically specific albedo estimates from MODIS (Table 1). Although *Myhre et al.* [2005] also used MODIS albedo data and a radiative transfer model to estimate TOA direct radiative effects of anthropogenic land cover changes, they reported a much weaker cooling effect (-0.09 W m^{-2}) than obtained by previous studies or this study. Their lower estimate of cooling derived from a relatively low surface albedo reported for snow-free cropland (0.14 to 0.17) combined with an imposed constraint on the change in surface albedo from preagricultural land cover to cropland [*Myhre et al.*, 2005]. Removing this constraint yielded a stronger TOA radiative forcing

Figure 3. Spatial patterns of (a, c, and e) albedo change and (b, d, and f) radiative forcing in December-January-February (Figures 3a and 3b), June-July-August (Figures 3c and 3d), and annual (Figures 3e and 3f) due to historical land cover change from 1700 to 2005 estimated from average of different data set combinations.

of $-0.14\,\mathrm{W\,m^{-2}}$. In comparison, *Betts et al.* [2007] reported a 1750–1990 radiative forcing from surface albedo change of $-0.20\,\mathrm{W\,m^{-2}}$, stronger than our study and double the best estimate provided by *Myhre et al.* [2005], and accounting for 75% of the total net cooling effect of anthropogenic land cover change which also included effects on evaporation, roughness, clouds, and longwave radiation.

The majority of past studies including those synthesized in the IPCC Fourth Assessment Report (2007) [*IPCC*, 2007] assumed geographically homogeneous albedo values for different land cover types. This assumption of geographically homogeneous albedo misses the regional and seasonal detail that emerges from variation in plant species, soil types and conditions, and land use practices, all of which are implicitly included with the more direct, geospatial application of remote sensing performed here. Some previous studies also only addressed conversion to croplands, missing conversion to pasture, and other land uses. The approach presented here considers a wider range of conversion types along with within-class variability in the albedo assigned to each land cover class through reliance on the LUMs. These new LUMs provide unique regional specificity of the albedo for each land cover type on local soils and for pure pixels, meaning those composed of only one land cover type. It is expected that this data set would better reflect the true albedo impacts of in situ land cover changes and should be possible to incorporate these LUM results to adjust global parameterizations typically applied in land surface models.

In addition to the new, MODIS-based albedo estimates used in this study, radiative forcing in our study derives from the newer LUH historical land use reconstruction [*Hurtt et al.*, 2006, 2011] (Table 1).

Table 1. Global Radiative Forcing From Anthropogenic Land Cover Change for a Range of Studies[a]

Source	LCC RF (W m^{-2})	Method	LCC Source	LCC Attribute	Albedo Source/Attribute	Time Period
Myhre et al. [2005]	−0.09	Atmospheric radiative transfer model	PV and MODIS	MODIS prescribed	MODIS look-up table	PV–present
Brovkin et al. [2006]	−0.14	Six EMICs: some with ET, precipitation, snowmelt, roughness, and cloud responses	PV (RF99) and modeled M83 or DT94	Grassland characteristics assumed representative of cropland values	EMIC default albedo values for trees and grass	1700–1992
This study [2014]	−0.15	Direct effect of SW radiation only with radiative kernel using different data set combinations	LUH	18 IGBP land cover classes	MODIS look-up maps	1700–2005
Pongratz et al. [2009]	−0.18	JSBACH land and ECHAM5 climate model without ET and roughness impacts	PV and P08	Three agriculture classes (crop, C3 pasture, and C4 pasture) and 11 natural vegetation classes	Prescribed albedo and phenology	1700–1992
Betts et al. [2007]	−0.20	HadAM3 AGCM: ET and roughness included	PV (RF99) and WHS85 adjusted by KG01 and RF99	53 cover types including 11 crop classes and 7 pasture/grazing classes	Albedo assigned based on local land cover type	1750–1990
IPCC AR4 [2007]	−0.08 to −0.50	Various	Various	Various	Various	
IPCC AR5 [2013]	−0.05 to −0.25	Various	Various	Various	Various	

[a]LCC = land cover change, IGBP = International Geosphere-Biosphere Programme, MODIS = Moderate Resolution Imaging Spectroradiometer, EMIC = Earth System Models of Intermediate Complexity, IPCC AR4 = Intergovernmental Panel on Climate Change Fourth Assessment Report, AGCM = atmospheric general circulation model, HadAM3 = Hadley Centre Coupled Model version 3, ESM = Earth System Model, RF = radiative forcing, SW = shortwave, ET = evapotranspiration, PV = potential vegetation based on biogeographical associations to current climate, LUH = Land use Harmonization data set of *Hurtt et al.* [2006, 2011], RF99 = historical croplands reconstructed from *Ramankutty and Foley* [1999], KG01 = land cover change from the HYDE data set of *Goldewijk* [2001], P08 = land cover reconstruction based on croplands (RF99) and pasturelands (KG01), DT94 = land cover data set of *DeFries and Townshend* [1994], M83 = land cover data set of *Matthews* [1983], and WHS85 = land cover data set of *Wilson and Henderson-Sellers* [1985].

Several previous studies relied on potential vegetation maps to describe historical land cover. In contrast, the land use harmonization product combines multiple sources of evidence (e.g., data sets, models, and countrywide statistical data), including data on harvest removals and subsequent regrowth, to estimate historical land cover in greater detail. This is currently the most comprehensive product describing land change of which we are aware and has been used in the IPCC Fifth Assessment Report [*IPCC*, 2013].

Overall, however, there appears to have been considerable narrowing in the range of albedo radiative forcing estimates in recent studies, compared to the wide range of estimates presented in IPCC Fourth Assessment Report [*IPCC*, 2007]. Since 2007, this study and three other studies [*Betts et al.*, 2007; *Brovkin et al.*, 2006; *Pongratz et al.*, 2009] have converged on radiative forcing values between −0.14 and −0.20 W m^{-2}. The adoption of more consistent remote sensing estimates of albedo coupled with improved land use reconstructions may thus be removing a central uncertainty to global climate forcing.

This study quantified the direct consequences of anthropogenic land use change solely on albedo and TOA radiative forcing. It is important to note that the range of climate relevant effects of anthropogenic land cover change includes changes in albedo, evapotranspiration, outgoing longwave radiation, and surface roughness, with albedo effects dominating at the global scale [*Betts et al.*, 2007]. The direct albedo effect of anthropogenic land cover change may be amplified by positive feedback involving sea ice, water vapor, and possibly cloud cover, although the cloud feedback is less clear because of countervailing influences of lower evapotranspiration which reduces cloud cover but cooler surfaces which can increase cloud cover

[*Brovkin et al.*, 2006]. In addition, general circulation models show large teleconnections that lead to significant warming over land and ocean regions, remote from the land use changes themselves, and these teleconnections can offset the direct effects of surface albedo change [*Zhao et al.*, 2001]. Net radiative impacts of land cover change-induced changes in evapotranspiration are complicated by a variety of responses that can have opposite signs including higher surface temperatures and associated increase in outgoing longwave radiation, decreased cloud cover, and associated decrease in planetary albedo but also decreased absorption of outgoing longwave radiation from the surface, as well as the water vapor feedback and increased evaporation over oceans. Historical anthropogenic landcover change has predominantly involved deforestation in temperate and some boreal regions, where evapotranspiration effects are second order relative to albedo impacts [*Betts et al.*, 2007], although this may not be true with the present-day tropical deforestation. A more comprehensive, model-based analysis incorporating the albedo LUMs introduced here would be required to quantify both the direct and indirect effects of surface albedo change on global radiative forcing and the climate system.

References

Bala, G., K. Caldeira, M. Wickett, T. J. Phillips, D. B. Lobell, C. Delire, and A. Mirin (2007), Combined climate and carbon-cycle effects of large-scale deforestation, *Proc. Natl. Acad. Sci. U.S.A.*, *104*(16), 6550–6555.

Barnes, C. A., and D. P. Roy (2010), Radiative forcing over the conterminous United States due to contemporary land cover land use change and sensitivity to snow and interannual albedo variability, *J. Geophys. Res.*, *115*, G04033, doi:10.1029/2010JG001428.

Betts, R. A., P. D. Falloon, K. K. Goldewijk, and N. Ramankutty (2007), Biogeophysical effects of land use on climate: Model simulations of radiative forcing and large-scale temperature change, *Agric. For. Meteorol.*, *142*(2), 216–233.

Bonan, G. B. (2008), Forests and climate change: Forcings, feedbacks, and the climate benefits of forests, *Science*, *320*(5882), 1444–1449.

Brovkin, V., M. Claussen, E. Driesschaert, T. Fichefet, D. Kicklighter, M. F. Loutre, H. D. Matthews, N. Ramankutty, M. Schaeffer, and A. Sokolov (2006), Biogeophysical effects of historical land cover changes simulated by six Earth system models of intermediate complexity, *Clim. Dyn.*, *26*(6), 587–600.

DeFries, R. S., and J. R. G. Townshend (1994), NDVI-derived land cover classifications at a global scale, *Int. J. Remote Sens.*, *15*(17), 3567–3586.

Eidenshink, J. C., and J. L. Faundeen (1994), The 1 km AVHRR global land data set: First stages in implementation, *Int. J. Remote Sens.*, *15*(17), 3443–3462.

Fall, S., D. Niyogi, A. Gluhovsky, R. A. Pielke, E. Kalnay, and G. Rochon (2010), Impacts of land use land cover on temperature trends over the continental United States: Assessment using the North American Regional Reanalysis, *Int. J. Climatol.*, *30*(13), 1980–1993.

Foley, J. A., et al. (2005), Global consequences of land use, *Science*, *309*(5734), 570–574.

Friedl, M. A., et al. (2002), Global land cover mapping from MODIS: Algorithms and early results, *Remote Sens. Environ.*, *83*(1), 287–302.

Gao, F., T. He, Z. Wang, B. Ghimire, Y. Shuai, J. Masek, C. Schaaf, and C. Williams (2014), Multiscale climatological albedo look-up maps derived from moderate resolution imaging spectroradiometer BRDF/albedo products, *J. Appl. Remote Sens.*, *8*(1), 15, doi:10.1117/1.JRS.8.083532.

Goldewijk, K. K. (2001), Estimating global land use change over the past 300 years: The HYDE database, *Global Biogeochem. Cycles*, *15*(2), 417–433, doi:10.1029/1999GB001232.

Hall, D. K., G. A. Riggs, V. V. Salomonson, N. E. DiGirolamo, and K. J. Bayr (2002), MODIS snow-cover products, *Remote Sens. Environ.*, *83*(1–2), 181–194.

Hurtt, G. C., S. Frolking, M. G. Fearon, B. Moore, E. Shevliakova, S. Malyshev, S. W. Pacala, and R. A. Houghton (2006), The underpinnings of land-use history: Three centuries of global gridded land-use transitions, wood-harvest activity, and resulting secondary lands, *Global Change Biol.*, *12*(7), 1208–1229.

Hurtt, G. C., et al. (2011), Harmonization of land-use scenarios for the period 1500–2100: 600 years of global gridded annual land-use transitions, wood harvest, and resulting secondary lands, *Clim. Change*, *109*(1–2), 117–161.

Intergovernmental Panel on Climate Change (IPCC) (2007), *Climate Change 2007: The Physical Science Basis, Contribution of Working Group I to the Fourth Assessment Report of the Intergovernmental Panel on Climate Change*, Cambridge Univ. Press, New York.

Intergovernmental Panel on Climate Change (IPCC) (2013), *Climate Change 2013: The Physical Science Basis, Contribution of Working Group I to the Fifth Assessment Report of the Intergovernmental Panel on Climate Change*, Cambridge Univ. Press, New York.

Kalnay, E., et al. (1996), The NCEP/NCAR 40-year reanalysis project, *Bull. Am. Meteorol. Soc.*, *77*(3), 437–471.

Kistler, R., et al. (2001), The NCEP-NCAR 50-year reanalysis: Monthly means CD-ROM and documentation, *Bull. Am. Meteorol. Soc.*, *82*(2), 247–268.

Lawrence, D. M., K. W. Oleson, M. G. Flanner, C. G. Fletcher, P. J. Lawrence, S. Levis, S. C. Swenson, and G. B. Bonan (2012), The CCSM4 land simulation, 1850–2005: Assessment of surface climate and new capabilities, *J. Clim.*, *25*(7), 2240–2260.

Matthews, E. (1983), Global vegetation and land use: New high-resolution data bases for climate studies, *J. Appl. Meteorol.*, *22*(3), 474–487.

Matthews, H. D., A. J. Weaver, M. Eby, and K. J. Meissner (2003), Radiative forcing of climate by historical land cover change, *Geophys. Res. Lett.*, *30*(2), 1055, doi:10.1029/2002GL016098.

Myhre, G., and A. Myhre (2003), Uncertainties in radiative forcing due to surface albedo changes caused by land-use changes, *J. Clim.*, *16*(10), 1511–1524.

Myhre, G., M. M. Kvalevag, and C. B. Schaaf (2005), Radiative forcing due to anthropogenic vegetation change based on MODIS surface albedo data, *Geophys. Res. Lett.*, *32*, L21410, doi:10.1029/2005GL024004.

Pinty, B., A. Lattanzio, J. V. Martonchik, M. M. Verstraete, N. Gobron, M. Taberner, J. Widlowski, R. E. Dickinson, and Y. Govaerts (2005), Coupling diffuse sky radiation and surface albedo, *J. Atmos. Sci.*, *62*(7), 2580–2591.

Pongratz, J., T. Raddatz, C. H. Reick, M. Esch, and M. Claussen (2009), Radiative forcing from anthropogenic land cover change since AD 800, *Geophys. Res. Lett.*, *36*, L02709, doi:10.1029/2008GL036394.

Pongratz, J., C. H. Reick, T. Raddatz, and M. Claussen (2010), Biogeophysical versus biogeochemical climate response to historical anthropogenic land cover change, *Geophys. Res. Lett.*, *37*, L08702, doi:10.1029/2010GL043010.

Ramankutty, N., and J. A. Foley (1999), Estimating historical changes in global land cover: Croplands from 1700 to 1992, *Global Biogeochem. Cycles*, *13*(4), 997–1027, doi:10.1029/1999GB900046.

Randerson, J. T., et al. (2006), The impact of boreal forest fire on climate warming, *Science*, *314*(5802), 1130–1132.

Rienecker, M. M., et al. (2011), MERRA: NASA's modern-era retrospective analysis for research and applications, *J. Clim.*, *24*(14), 3624–3648.

Román, M. O., C. B. Schaaf, P. Lewis, F. Gao, G. P. Anderson, J. L. Privette, A. H. Strahler, C. E. Woodcock, and M. Barnsley (2010), Assessing the coupling between surface albedo derived from MODIS and the fraction of diffuse skylight over spatially-characterized landscapes, *Remote Sens. Environ.*, *114*(4), 738–760.

Schaaf, C. B., et al. (2002), First operational BRDF, albedo nadir reflectance products from MODIS, *Remote Sens. Environ.*, *83*(1–2), 135–148.

Shell, K. M., J. T. Kiehl, and C. A. Shields (2008), Using the radiative kernel technique to calculate climate feedbacks in NCAR's community atmospheric model, *J. Clim.*, *21*(10), 2269–2282.

Soden, B. J., I. M. Held, R. Colman, K. M. Shell, J. T. Kiehl, and C. A. Shields (2008), Quantifying climate feedbacks using radiative kernels, *J. Clim.*, *21*(14), 3504–3520.

Steffen, W. L., et al. (2005), *Global Change and the Earth System: A Planet Under Pressure*, Springer, Berlin.

Turner, B. L., E. F. Lambin, and A. Reenberg (2007), The emergence of land change science for global environmental change and sustainability, *Proc. Natl. Acad. Sci. U.S.A.*, *104*(52), 20,666–20,671.

Wilson, M. F., and A. Henderson-Sellers (1985), A global archive of land cover and soils data for use in general circulation climate models, *J. Climatol.*, *5*(2), 119–143.

Zhao, M., A. J. Pitman, and T. Chase (2001), The impact of land cover change on the atmospheric circulation, *Clim. Dyn.*, *17*(5–6), 467–477.